In situ x-ray reflectivity and grazing incidence x-ray diffraction study of $L\,1_0$ ordering in ^{57}Fe/Pt multilayers

2009 J. Phys.: Condens. Matter 21 186002

(http://iopscience.iop.org/0953-8984/21/18/186002)

J. Phys.: Condens. Matter **21** (2009) 186002 (8pp) doi:10.1088/0953-8984/21/18/186002

In situ x-ray reflectivity and grazing incidence x-ray diffraction study of $L1_0$ ordering in ^{57}Fe/Pt multilayers

V Raghavendra Reddy[1,4], Ajay Gupta[1], Anil Gome[1], Wolfram Leitenberger[2] and U Pietsch[3]

[1] UGC-DAE Consortium for Scientific Research, University Campus, Khandwa Road, Indore-452 017, India
[2] Institute of Physics, University of Potsdam, 14469 Potsdam, Germany
[3] Physics Department, University of Siegen, D-57068 Siegen, Germany

E-mail: vrreddy@csr.ernet.in and varimalla@yahoo.com

Received 22 November 2008, in final form 13 March 2009
Published 31 March 2009
Online at stacks.iop.org/JPhysCM/21/186002

Abstract

In situ high temperature x-ray reflectivity and grazing incidence x-ray diffraction measurements in the energy dispersive mode are used to study the ordered face-centered tetragonal (fct) $L1_0$ phase formation in [Fe(19 Å)/Pt(25 Å)]$_{\times 10}$ multilayers prepared by ion beam sputtering. With the *in situ* x-ray measurements it is observed that (i) the multilayer structure first transforms to a disordered FePt and subsequently to an ordered fct $L1_0$ phase, (ii) the ordered fct $L1_0$ FePt peaks start to appear at 320 °C annealing, (iii) the activation energy of the interdiffusion is 0.8 eV and (iv) ordered fct FePt grains have preferential out-of-plane texture. The magneto-optical Kerr effect and conversion electron Mössbauer spectroscopies are used to study the magnetic properties of the as-deposited and 400 °C annealed multilayers. The magnetic data for the 400 °C annealed sample indicate that the magnetization is at an angle of ∼50° from the plane of the film.

(Some figures in this article are in colour only in the electronic version)

1. Introduction

Due to their large magnetic anisotropy values ($K_u \sim 10^7$ erg cm^{-3}) the equiatomic FePt, CoPt and FePd alloy thin films have been of considerable research interest. The transformation of the disordered face-centered cubic (fcc) phase to the ordered face-centered tetragonal (fct) $L1_0$ phase has been attributed to be the reason for the high magnetic anisotropy [1]. Particularly, FePt thin films with $L1_0$ structure is a potential material for magnetic recording media, especially perpendicular media where the *c*-axis is oriented out-of-plane. The desired $L1_0$ phase is achieved by post annealing of the as-prepared samples at high temperatures. However, concurrently with $L1_0$ phase formation, high temperature annealing treatment also causes particle growth and coalescence, which may adversely affect the magnetic properties. Many attempts were made to obtain the $L1_0$ FePt phase at relatively lower temperatures [2–6]. A significant reduction in the temperature is observed with thermal annealing of Fe/Pt multilayer structures. The enhanced ordering process in the multilayers with thermal annealing is attributed to be due to rapid interdiffusion at the Fe/Pt interfaces. Because of the interdiffusion various phases of FePt namely, cubic FePt, tetragonal FePt, Fe rich Pt and Pt rich Fe are expected to form. It is therefore interesting and necessary to study structural transformation with thermal annealing in multilayers to correlate the observed magnetic properties. The other important aspect of $L1_0$ FePt material is the development of out-of-plane texture [7], which is essential from the application point of view based on perpendicular magnetic anisotropy. Therefore, it is necessary to study phase formation, texture etc, with thermal annealing of multilayers. Several studies using techniques like x-ray, Mössbauer, TEM etc, are reported with an aim to elucidate the structural evolution with thermal annealing of multilayers [4, 6, 8].

[4] Author to whom any correspondence should be addressed.

However, no *in situ* x-ray studies are reported in literature with thermal annealing of Fe/Pt multilayers which can give information regarding the development of various phases, texture etc, as a function of annealing temperature and time. In the present work, we have attempted to study the issues like intermixing, evolution of phases, texture etc, with the thermal annealing of equiatomic Fe/Pt multilayers using *in situ* x-ray scattering measurements with synchrotron radiation. Further, the *in situ* x-ray scattering in two geometries namely, in-plane and out-of-plane simultaneously is expected to give unambiguous information about texture. The observations of the x-ray measurements are supported by the magnetic measurements namely, the magneto-optical Kerr effect and conversion electron Mössbauer spectroscopy.

2. Experimental details

$[^{57}\text{Fe}(19\ \text{Å})/\text{Pt}(25\ \text{Å})]_{\times 10}$ multilayers were deposited on Si(111) substrate using ion beam sputtering [8]. It may be noted that the thickness values of Fe and Pt are selected so as to have the equal number of atoms. A beam of argon ions was used to sputter ^{57}Fe-enriched Fe and Pt targets using Kaufman type hot-cathode ion source. A base vacuum of 1×10^{-7} Torr was achieved before deposition. The targets were mounted on rotary motion feed through to switch over from Fe to Pt in order to deposit alternate layers. *In situ* high temperature x-ray reflectivity (XRR) and grazing incidence x-ray diffraction (GIXRD) measurements are carried out using EDXRD beam line of BESSY-II synchrotron source [9]. Rontec x-flash detectors are used to measure the scattered x-rays, while the x-rays were allowed to fall on the sample at a grazing angle of 0.5°. Measurements are done *in situ* as a function of annealing temperature inside a vacuum furnace evacuated with a turbomolecular pump to a vacuum of the order of $\sim 10^{-5}$ mbar. Two sets of *in situ* x-ray scattering experiments are carried out. In the first experiment, *in situ* XRR and in-plane GIXRD patterns are recorded simultaneously using two detectors to study the intermixing and the phases developed with the thermal annealing. The first detector is kept vertically above the direct beam and the second detector is kept in the plane of the incident beam to cover the angles of interest for measuring XRR and in-plane GIXRD, respectively. In the second experiment *in situ* GIXRD measurements are carried out in two geometries with (i) the scattering vector in the film plane and (ii) scattering vector out-of-the-film plane (henceforth designated as in-plane and out-of-plane GIXRD patterns) simultaneously to study texture etc. The detector used for measuring XRR in the first experiment is used to measure out-of-plane GIXRD data. At each temperature the data was collected for 300 s and roughly the time taken to reach and stabilize at a given temperature was about 120 s. The position of the detectors (i.e., the angle of scattering) is calibrated by recording the NaCl diffraction pattern and the measured energy dispersive x-ray data is normalized with the incident BESSY-II spectrum [9]. The resolution of the detectors used was $\Delta E/E = \Delta q/q \sim 10^{-2}$ and the typical width of the peaks observed for NaCl powder was about 0.03 Å^{-1} that gives the instrumental resolution. *Ex situ* XRR and GIXRD

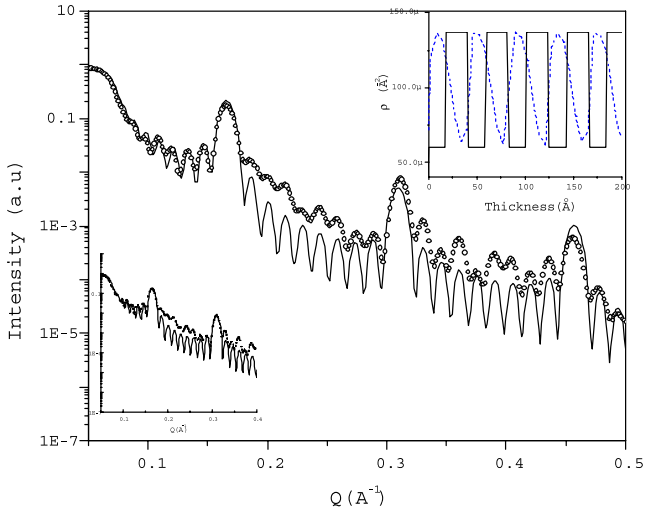

Figure 1. XRR pattern of pristine $[^{57}\text{Fe}(19\ \text{Å})/\text{Pt}(25\ \text{Å})]_{\times 10}$ multilayer measured in the angle dispersive mode. The solid line shows the best fit to the data. The top inset shows the corresponding energy density profile (dotted line) and simulated profile with sharp interfaces (solid line). The bottom inset shows the fit to XRR data with Fe/FePt/Pt structure.

measurements of the as-deposited (pristine) sample are carried out using a Bruker D8-Discover system. Conversion electron Mössbauer spectroscopy (CEMS) is recorded using the conventional PC-based Mössbauer spectrometer in the back scattering geometry with home made continuous gas flow detector using 95%He+5%CH_4 gas mixture. The in-plane and out-of-plane M–H loops at room temperature are measured in longitudinal and polar geometries respectively using the magneto-optical Kerr effect (MOKE) system equipped with an intensity stabilized He–Ne laser, Glan–Taylor prisms, a Stanford lock-in amplifier, photo-elastic modulator, silicon photodiode and a M/s Janis 7 T superconducting magnet (for high field measurements)/$\sim$2 kOe electromagnet (for low field measurements).

3. Results and discussion

Figure 1 shows the XRR pattern of the pristine sample measured in the angle dispersive mode using lab source (Cu Kα). The Bragg peaks, up to third order in the XRR pattern, demonstrate the clear stratification in the as-deposited sample. The XRR patterns are fitted with Parratt formalism [10] and the obtained thickness values for the as-deposited film are 26.7±1 Å and 18.1±1 Å for Pt and Fe layers respectively and the bilayer periodicity is 44.8 Å. The inset of figure 1 shows the electron density profile (EDP) obtained from the fitting. From the obtained electron density profile (EDP) as shown in the inset of figure 1, it can be concluded that the interfaces are not sharp, but rather represent a very diffused compositional profile which is evidence of a strong intermixing at the interfaces in the pristine sample itself. As a result of this the sample consists of FePt alloy phase in addition to pure Fe, Pt layers. The XRR pattern is also fitted by considering the FePt alloy at both interfaces (i.e., Fe on Pt and Pt on Fe)

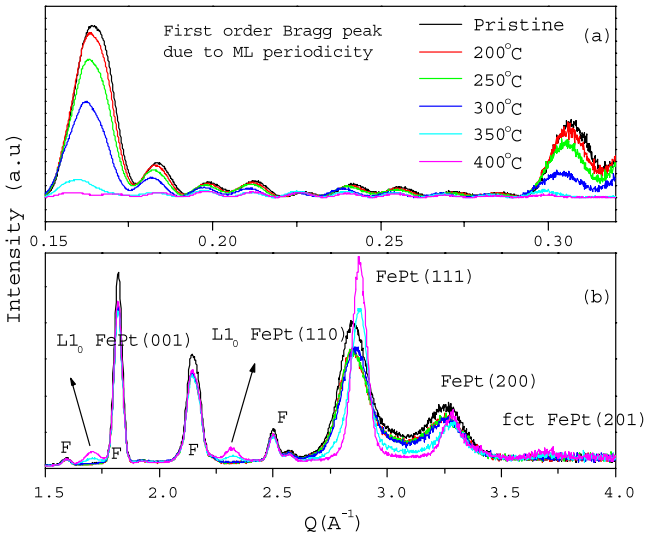

Figure 2. *In situ* high temperature (a) XRR patterns and (b) in-plane GIXRD patterns of $[^{57}\text{Fe}(19\ \text{Å})/\text{Pt}(25\ \text{Å})]_{\times 10}$ multilayer at the indicated temperatures measured in the energy dispersive mode. Peaks marked with 'F' represent the fluorescence lines from the sample.

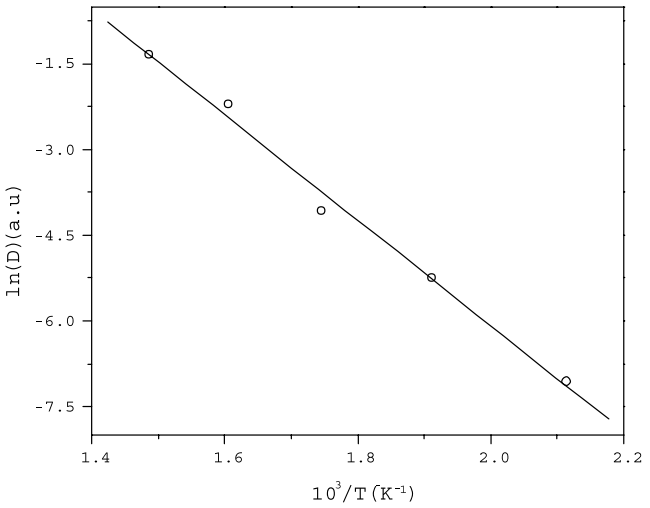

Figure 3. Relationship between $\ln(D)$ and $10^3/T$ of $[^{57}\text{Fe}(19\ \text{Å})/\text{Pt}(25\ \text{Å})]_{\times 10}$ multilayer obtained from *in situ* high temperature XRR measurements in the energy dispersive mode.

and is shown as the bottom inset of figure 1. One may note the improvement in the fitting around the second Bragg peak. This observation is further evidenced from the Mössbauer (figure 11) and energy dispersive GIXRD data (figure 4) of the pristine sample as discussed below. The angle dispersive data presented in figure 1 is further used to accurately cross check the calibration of the x-axis (i.e., scattering angle or 'Q' obtained from NaCl data) of the measured *in situ* energy dispersive XRR and GIXRD data.

Figures 2(a) and (b) show the *in situ* high temperature XRR and in-plane GIXRD patterns of the Fe/Pt multilayer at the indicated temperatures measured in the energy dispersive mode. In the XRR patterns of as-deposited film one can clearly see the first- and second-order Bragg peaks at 0.16

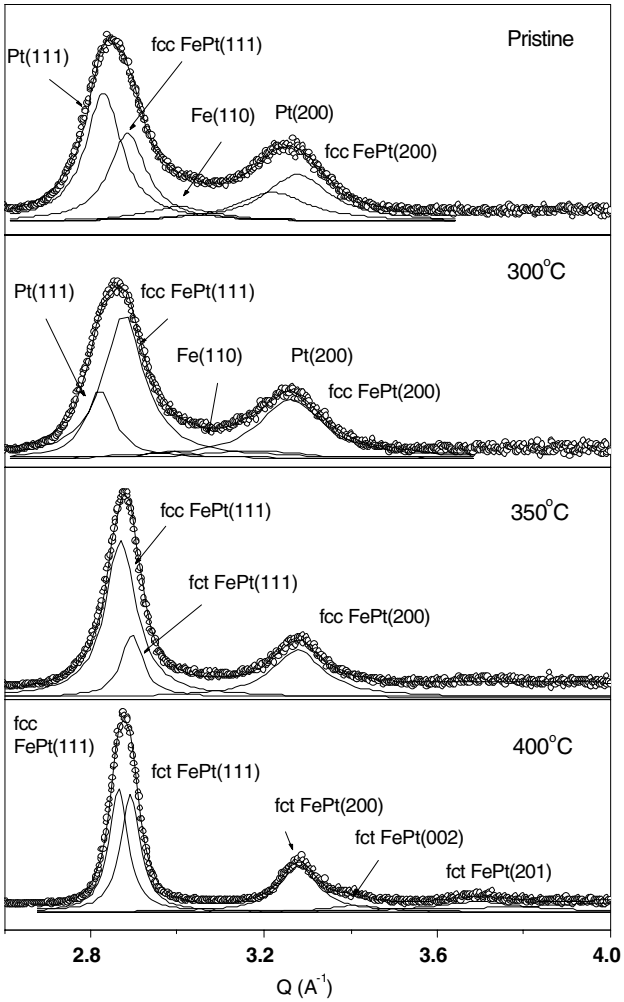

Figure 4. In-plane XRD patterns of $[^{57}\text{Fe}(19\ \text{Å})/\text{Pt}(25\ \text{Å})]_{\times 10}$ multilayer at the indicated temperatures measured in the energy dispersive mode showing the peaks from Pt, fcc FePt and Fe as a function of annealing temperature.

and 0.31 Å^{-1} due to multilayer periodicity. The intensity of the first-order Bragg peak is proportional to the square of the amplitude of the first Fourier component of the modulation composition and depends on the effective interdiffusivity of the multilayers. The intensity of the first-order Bragg peak of figure 2(a) is estimated to find out the activation energy of interdiffusion in Fe/Pt multilayers using the following equation

$$\ln\left(\frac{I(T)}{I(0)}\right) = -4\pi^2 n^2 L_{\text{d}}^2/\Lambda^2$$

where $I(T), I(0)$ are the intensity of the Bragg peak at temperature T and the pristine sample, 'n' is the order of Bragg peak, Λ is the bilayer periodicity, diffusion length $L_{\text{d}}^2 = 2Dt$, D is the diffusion coefficient and 't' is the annealing time [11]. The obtained 'D' values are used to find the activation energy (H_{e}) and pre-exponential factor (D_0) from the equation $D = D_0 \exp(-H_{\text{e}}/k_{\text{B}}T)$ as shown in figure 3. The obtained D_0 and H_{e} values are 2.3×10^{-15} m^2 s^{-1} and 0.80 ± 0.04 eV, respectively. The obtained activation energy matches well with the values determined in Fe/Pt multilayers using the Auger

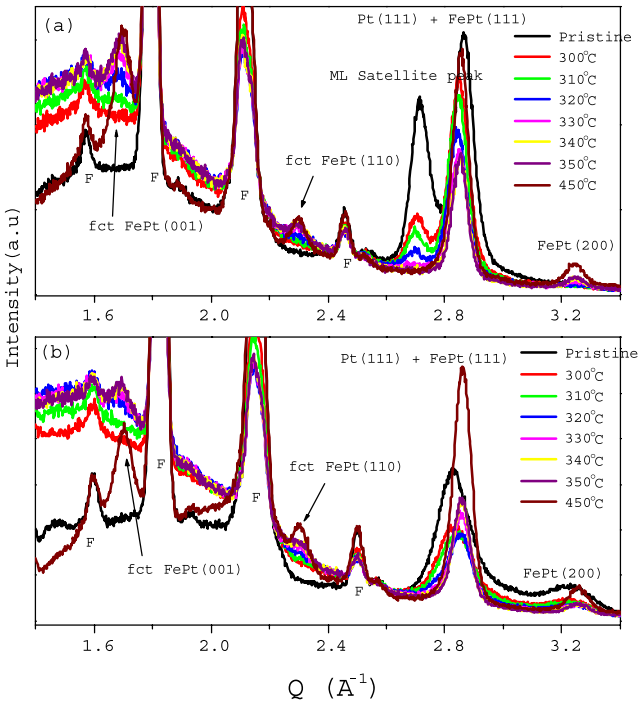

Figure 5. Energy dispersive *in situ* high temperature (a) out-of-plane GIXRD patterns of $[^{57}\text{Fe}(19\ \text{Å})/\text{Pt}(25\ \text{Å})]_{\times 10}$ multilayer showing the deterioration of multilayer structure characterized by the decrease in the intensity of multilayer satellite peak and development of fct $L1_0$ FePt peaks with the annealing at the indicated temperatures, (b) in-plane GIXRD pattern of the $[^{57}\text{Fe}(19\ \text{Å})/\text{Pt}(25\ \text{Å})]_{\times 10}$ multilayer. Peaks marked with 'F' represent the fluorescence lines from the sample.

electron spectroscopy (AES) depth profiling method [12] and also the obtained D_0 and H_e correlate well with the data of multilayers reported in the literature (figure 10 of [11]).

Figure 2(b) shows the in-plane energy dispersive GIXRD pattern of Fe/Pt ML as a function of annealing temperature consisting of structural peaks of the sample and various fluorescence lines (marked with 'F'). Peaks corresponding to ordered fct $L1_0$ FePt (001) and (110) at 1.69 and 2.31 Å^{-1} respectively are clearly observed at and above 350 °C annealing temperature, indicating that the fcc to fct transformation is taking place between 300 and 350 °C temperatures. These results match with our earlier *ex situ* x-ray studies of the same Fe/Pt multilayer [6]. The detailed fitting of the in-plane GIXRD data is shown in figure 4. One can clearly resolve the peak at about 2.8 Å^{-1} of the pristine sample into two sharp peaks corresponding to Pt(111) and fcc FePt(111) at 2.829 ± 0.002 and 2.885 ± 0.003 Å^{-1} respectively and a broad peak at 3.004 ± 0.014 Å^{-1} corresponding to Fe(110). The shift of Pt(111) peak to a higher angle as compared to bulk Pt(111) is similar to the case of sputter deposited Co/Au multilayers [13], which can be understood as following. As the atomic radii for Fe and Pt are different, $r_{Fe} = 1.24$ Å and $r_{Pt} = 1.39$ Å, there will be a strain induced within the planes which will be constrictive for the Pt planes and tensile for the Fe planes. It may be noted here that the observed diffraction data of the pristine sample supports the observations of XRR data (figure 1) indicating that the as-deposited sample consists of FePt alloy phase formation at the interfaces of Fe and Pt layers. Similarly the other peak at ~3.22 Å^{-1} is resolved into two peaks corresponding to Pt(200) and fcc FePt(200) peaks at 3.220 ± 0.057 and 3.277 ± 0.020 Å^{-1}, respectively. Therefore, from the above x-ray analysis, one can model the structure of as-deposited Fe/Pt ML as [Fe/fcc FePt/Pt]. As shown in figure 4, with an increase in the annealing temperature peaks corresponding to Pt(111), Fe(110) are reducing in intensity and the intensity of FePt phase is increasing. At 350 °C peak corresponding to fct FePt(111) is seen with an increase in the intensity with further increase in the temperature.

Further, the second experiment is carried out with 10 °C interval across the transition temperature (i.e., between 300 and 400 °C) by measuring *in situ* in-plane and out-of-plane GIXRD data as discussed in section 2. Figure 5 shows the out-of-plane and in-plane GIXRD patterns at the indicated temperatures. Peaks marked with 'F' represent fluorescence lines from the sample in figure 5. For the sake of clarity, the patterns close to the transition temperature only are shown in figure 5. The clear distinction between the two patterns is the presence of sharp peak at about ~2.7 Å^{-1} in the out-of-plane geometry, which is attributed to be the satellite peak due to multilayer periodicity. Because the origin of the satellite peak is the periodicity of the bilayers in the vertical direction, the satellite peak is absent in the in-plane geometry where the scattering vector is in the film plane. Such multilayer satellite peaks are reported in literature with θ–2θ scans because of strong structural coherence between individual layers of the multilayers [14, 15]. To resolve the issue further, the out-of-plane GIXRD data of the pristine sample is measured in the angle dispersive mode using lab source as shown in figure 6(a). The GIXRD data is recorded at different angles of incidence (α_i) and the position and width of the (111) peak is evaluated and is shown in figures 6(b) and (c), respectively. The separation of the main peak i.e., (111) and the satellite peak is also estimated as shown in figure 6(d). The data point at $\alpha_i = 20°$ corresponds to θ–2θ scan. The decrease in the position of the (111) peak as α_i is increased can be understood in terms of the angle of refraction effects [16]. The angular shift due to refraction caused by the penetration of the x-ray beam is approximately estimated as $\Delta 2\theta = \alpha_i - (\alpha_i^2 - \alpha_C^2)^{1/2}$ where α_C is the critical angle [16]. The variation of the peak position observed in the present study (i.e., figure 6(b)) is fitted with the above equation (with α_C as the fitting parameter). The solid line in figure 6(b) shows the best fit to the data and the obtained value of α_C is ~0.74° which closely matches with the critical angel of the upper layer (i.e., Pt). As α_i increases, the separation of the main and the satellite peak is increasing (figure 6(d)). This is due to the fact that as the angle increases the periodicity of the compositional modulation along the 'Q' (i.e., momentum transfer vector) decreases and hence the separation increases. The (111) peak width (figure 6(c)) is observed to decrease with the angle of incidence indicating that the coherence length is increasing in the vertical direction with the angle of incidence. But, at the grazing incidences since the momentum transfer vector is not exactly perpendicular to the surface of the sample, it is expected that the coherence

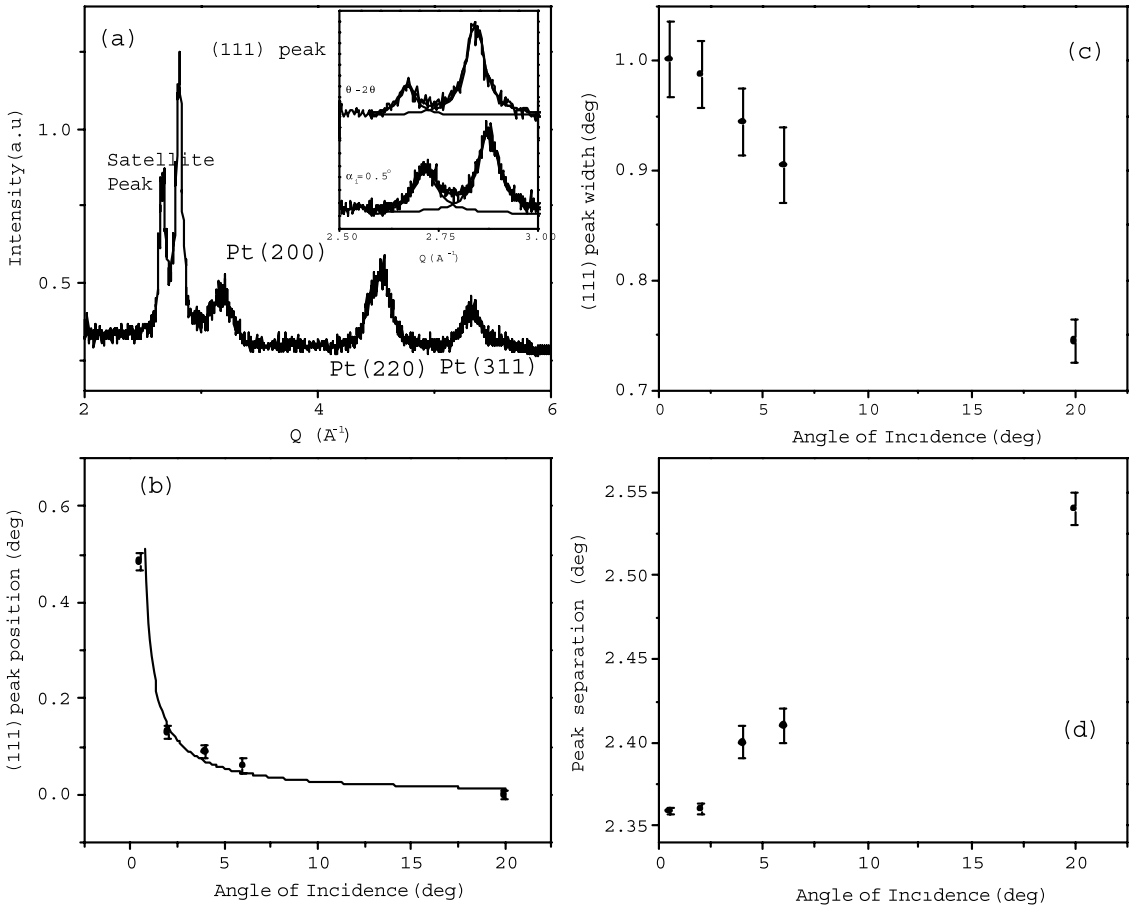

Figure 6. (a) GIXRD spectra of pristine $[^{57}\text{Fe}(19\ \text{Å})/\text{Pt}(25\ \text{Å})]_{\times 10}$ multilayer measured in the angle dispersive mode; (b), (c) and (d) show the results obtained from depth resolved GIXRD measurement at different angles of incidence (α_i). The inset of (a) shows the GIXRD pattern at $\alpha_i = 0.5°$ incidence and θ–2θ scan.

length should be more (i.e., peak width should be small) as compared to when the momentum transfer vector is exactly perpendicular to the surface of the film. This indicates that in the pristine Fe/Pt ML, the grains have more coherence in the vertical direction as compared to the in-plane coherence i.e., the crystallites are elongated vertically in the sample. This is further evidenced by calculating the crystalline size using Debye–Scherrer formula [17] from the width of the peak at $\sim$2.8 Å^{-1} in the *in situ* in-plane and out-of-plane GIXRD data (figure 5) of the pristine sample. The obtained crystalline size values after subtracting the instrumental broadening are observed to be more in out-of-plane geometry as compared to in-plane geometry. This indicates that the grains have more coherence in the vertical direction as compared to the in-plane direction.

One can clearly see from figure 5(a), as the annealing temperature is increased, the multilayer satellite peak intensity is reducing and reaching to zero at about 320 °C indicating the gradual mixing at the interfaces leading to the formation of FePt alloy. The high angle out-of-plane x-ray patterns are fitted with the superlattice refinement (SUPREX) program [14, 15] with the interdiffusion model [18]. Figure 7 shows the high angle x-ray profiles along with the fitted data. The obtained thickness parameters from the SUPREX fitting closely match the layer thickness values obtained from XRR (figure 1). Keeping all the parameters fixed, the interface width (interface width of A–B and B–A are assumed to be equal) was varied to fit the data of the annealed spectra. The interface width was observed to increase from 3.42 to about 22.85 ML with the annealing at 320 °C. It is observed that as the annealing temperature increases further, the satellite peak disappears. The peaks corresponding to the ordered fct $L1_0$ are seen starting from 320 °C annealing temperature. Therefore, even though the mixing at the interface (indicated by the intensity reduction of the satellite peak) is taking place gradually, the peaks corresponding to the ordered fct $L1_0$ are seen clearly starting only from 320 °C annealing temperature. This observation indicates that the multilayer structure first converts into a disordered FePt phase and subsequently converts into an ordered FePt phase. The obtained interface width is used to estimate diffusion coefficient (D) from the equation $D(T) = (\sigma_T^2 - \sigma_0^2)/2t$, where σ_T and σ_0 are the interface width values at a given temperature and of the pristine sample, respectively [19]. The activation energy (H_e) of interdiffusion is obtained as 1.1 ± 0.15 eV from the slope of ln D and $1/T$ as shown in figure 8. The obtained value of H_e matches closely with the value obtained from the low angle satellite about the (000) x-ray peak i.e, first-order Bragg peak due to multilayer periodicity as shown in figure 3.

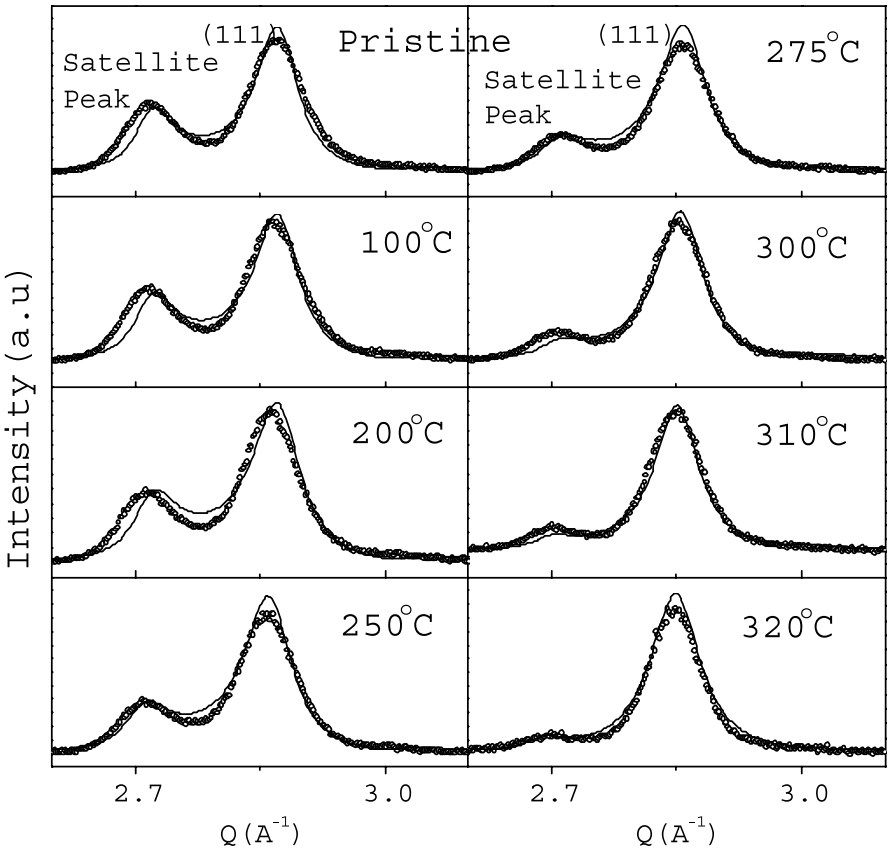

Figure 7. Out-of-plane GIXRD data of $[^{57}\text{Fe}(19\ \text{Å})/\text{Pt}(25\ \text{Å})]_{\times 10}$ multilayer showing the reduction in the intensity of the multilayer satellite peak with temperature. The solid line represents the fit to the data with the SUPREX program.

Figure 9 shows the '*d*' values of fct FePt(001) peak represented as $d(001)$ obtained from both in-plane and out-of-plane GIXRD data of figure 5. It may be noted that $d(001)$ becomes almost equal above 400 °C annealing. However, the variation of $d(001)$ is quite different during the initial stages of fct FePt phase formation indicating some structural relaxation is taking place during the ordering due to the presence of strains. The rapid decrease of in-plane $d(001)$ indicates the presence of tensile stress. Whereas, the width of the peak is observed to decrease continuously in both the geometries indicating the grain growth with the annealing as expected.

The texture of fct FePt is obtained by comparing $I_{(001)}/I_{(110)}$ i.e. the intensity ratio of fct FePt(001) to fct FePt(110) peaks at ∼1.69 and 2.31 Å^{-1} respectively in both out-of-plane and in-plane geometries at a given temperature. For example, the value of $I_{(001)}/I_{(110)}$ at 400 °C from the out-of-plane GIXRD data is about 2.41 and whereas the value of the same is about 1.55 from the in-plane GIXRD data. This indicates that the fct FePt grains have a slight preferential orientation along (001) direction. This observation is further evidenced from the magnetic measurements i.e., Mössbauer and MOKE as discussed below. The magnetic measurements are carried out on two samples i.e., the pristine (as-deposited) film and the film annealed at 400 °C for 90 min in a vacuum better than 1×10^{-6} Torr.

Figure 10 shows the room temperature M–H loops of the pristine and 400 °C annealed samples measured with MOKE

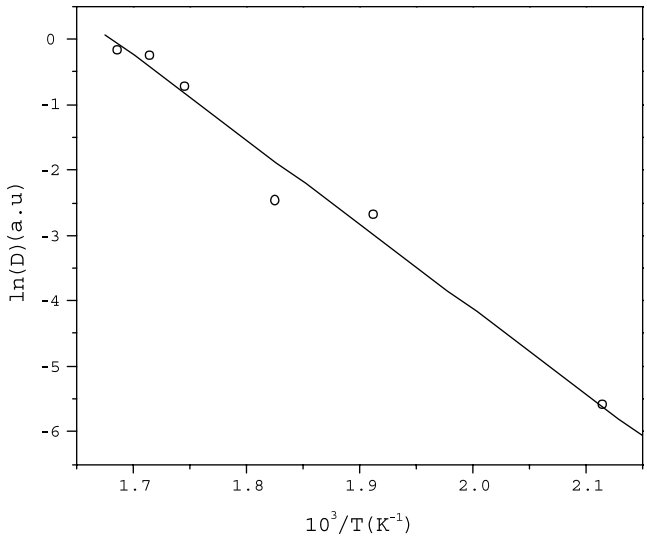

Figure 8. Relationship between $\ln(D)$ and $10^3/T$ of $[^{57}\text{Fe}(19\ \text{Å})/\text{Pt}(25\ \text{Å})]_{\times 10}$ multilayer obtained from *in situ* high temperature out-of-plane GIXRD measurements in the energy dispersive mode.

in longitudinal and polar geometries (henceforth designated as L-MOKE and P-MOKE). The measurements in polar geometry are carried out using a superconducting magnet with near normal incidence of laser light. The data presented in figure 10(b) is after subtracting the window contribution of the

Table 1. Hyperfine parameters obtained from the Mössbauer spectra of 400 °C annealed film.

Phase	Width (mm s^{-1})	Area (%)	Isomer shift (mm s^{-1})	Quadrupole splitting (mm s^{-1})	BHF (T)	$A23$
fct	0.385 ± 0.013	65.1	0.341 ± 0.005	0.338 ± 0.009	28.77 ± 0.024	1.627 ± 0.03
fcc	0.425 ± 0.027	34.9	0.236 ± 0.009	-0.090 ± 0.02	29.44 ± 0.046	1.627 ± 0.03

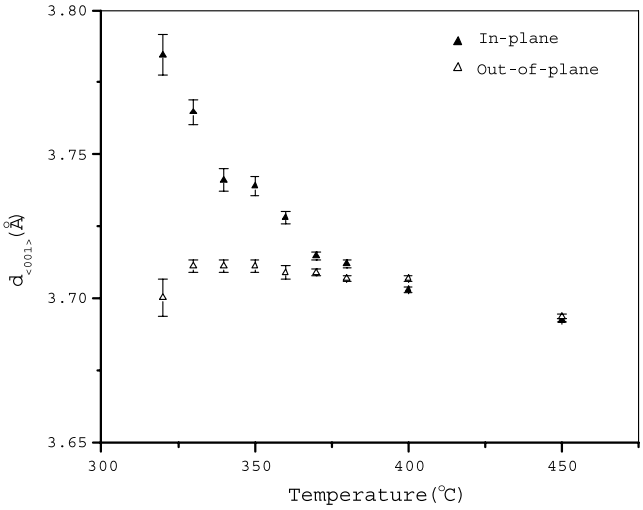

Figure 9. Variation of in-plane and out-of-plane 'd' spacing of the fct FePt(001) peak with annealing.

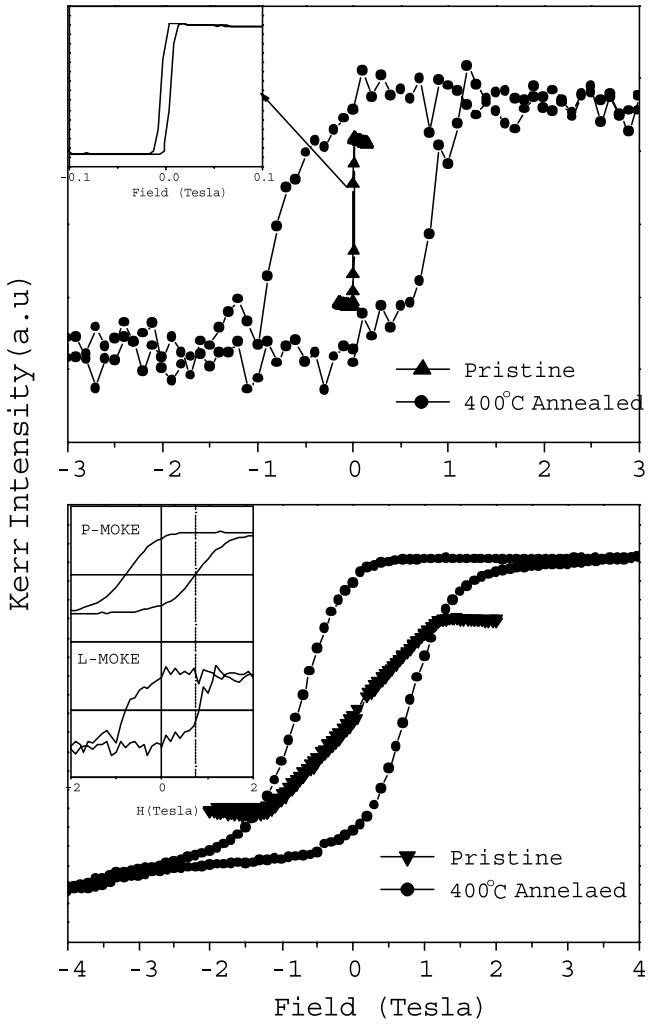

Figure 10. (a) In-plane and (b) out-of-plane magnetization data of pristine and 400 °C annealed $[^{57}\text{Fe}(19\ \text{Å})/\text{Pt}(25\ \text{Å})]_{\times 10}$ multilayers measured using MOKE in longitudinal and polar geometries, respectively. The inset of (a) represents the in-plane magnetization data of the pristine sample; (b) shows the in-plane and out-of-plane data of the 400 °C annealed sample showing H_c values.

superconducting magnet. The longitudinal MOKE data of as-deposited film is carried out using an electromagnet and that of 400 °C annealed film is carried out using a superconducting magnet. The noisy data of 400 °C film in the longitudinal direction is due to the low angle of incidence of the laser, which is restricted because of the magnet windows. The L-MOKE and P-MOKE data of the pristine sample clearly indicates the in-plane magnetization, which is expected. With the annealing at 400 °C, the observed coercivity (H_c) values from L- and P-MOKE measurements respectively are 0.81 and 0.75 T (as shown in inset of figure 10(b)). It may be noted that the MOKE measurements in longitudinal and polar geometries are sensitive to the in-plane and out-of-plane magnetization components [20]. The observation of slightly less H_c value in out-of-plane geometry (i.e., P-MOKE) indicates that the magnetization is oriented close to the film normal as compared to film plane. The actual orientation of magnetization with respect to the film normal i.e., (001) is obtained from Mössbauer measurements as discussed below.

Figure 11 shows the CEMS spectra of the pristine and 400 °C annealed samples. The Mössbauer spectrum of as-deposited film is fitted with the distribution of hyperfine fields, as the spectral lines are broad because of the distribution of hyperfine fields. An average hyperfine field of 24.7 T, which is considerably lower than the pure Fe layer hyperfine field (∼33 T), is observed in the as-deposited film. This is because the neighboring platinum atoms around iron atoms reduce the hyperfine field of Fe [21], as some amount of Pt is expected to diffuse into the Fe layer in the as-deposited film supporting the observations of x-ray measurements. As the spectral lines for the 400 °C annealed sample are observed to be sharp, the spectra are fitted as an overlap of two sextets for obtaining the hyperfine parameters. The best fit is obtained when the $A23$ parameter of both sextets is constrained to be equal. The obtained hyperfine parameters relative to natural iron are shown in table 1. The sextet with near zero quadrupole splitting is due to fcc FePt and the one with high quadrupole splitting is due to the ordered $L1_0$ fct FePt phase. The orientation of Fe average spin angle θ values with respect to the γ-direction (normal to the film plane) calculated from the area ratio of the second and third Mössbauer lines (i.e., $A23$) for

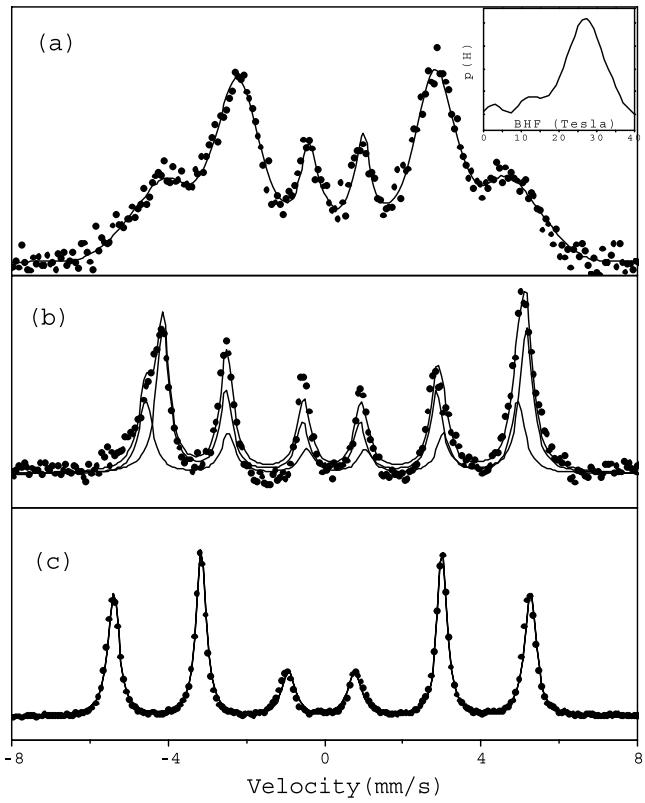

Figure 11. CEMS spectra of (a) pristine and (b) 400 °C annealed $[^{57}\text{Fe}(19\ \text{Å})/\text{Pt}(25\ \text{Å})]_{\times 10}$ multilayers and (c) ^{57}Fe enriched Fe foil. The solid line represents the best fit to the data. The inset of (a) shows the probability distribution of the hyperfine field.

as-deposited and 400 °C annealed sample are 90° and 40.5°, respectively [22]. These values indicate that the magnetization of the pristine film lies in the plane of the film and for 400 °C annealed film, the magnetization is rotated away from the film plane by an angle of ∼50°, which indicates a slight preferential orientation towards the surface normal i.e., (001) spin orientation. These observations match with MOKE and x-ray measurements as discussed above.

In conclusion the ordered fct $L1_0$ FePt phase formation from the thermal annealing of $[\text{Fe}(19\ \text{Å})/\text{Pt}(25\ \text{Å})]_{\times 10}$ multilayers is studied using *in situ* x-ray scattering measurements. It is observed that the ordered $L1_0$ phase forms at 320 °C and the multilayer structure first transforms into a disordered FePt and subsequently into an ordered FePt phase. Activation energy of 0.80 eV is obtained for the interdiffusion in Fe/Pt multilayers. Using x-ray measurements it is observed that the fct FePt grains have (001) texture supported by the magnetic measurement namely, Mössbauer and the magneto-optical Kerr effect.

Acknowledgment

The *in situ* x-ray studies are carried out at BESSY-II light source in the Indo-German project entitled 'Time resolved x-ray scattering using the energy dispersive beam line at BESSY-II/INUDS' sanctioned by DST, New Delhi.

References

[1] Ivanov O A, Solina L V and Demshina V A 1973 *Phys. Met. Metallogr.* **35** 81
[2] Maeda T, Kai T, Kikitsu A, Nagase T and Akiyama J-I 2002 *Appl. Phys. Lett.* **80** 2147
[3] Cellollada A, Weller D, Sticht J, Harp G R, Farrow R F C, Marks R F, Savoy R and Scott J C 1994 *Phys. Rev.* B **50** 3419
[4] Endo Y, Kikuchi N, Kitakami O and Shimada Y 2001 *J. Appl. Phys.* **89** 7065
[5] Kavita S, Reddy V R, Gupta A and Gupta M 2005 *Hyperfine Interact.* **160** 157
[6] Reddy V R, Kavita S and Gupta A 2006 *J. Appl. Phys.* **99** 113906
[7] Rasmussen P, Rui X and Shield J E 2005 *Appl. Phys. Lett.* **86** 19195
[8] Simopoulos A, Devlin E, Kostikas A, Jankowski A, Croft M and Tsakalakos T 1996 *Phys. Rev.* B **54** 9931
Liu J P, Luo C P, Liu Y and Sellmyer D J 1998 *Appl. Phys. Lett.* **72** 482
[9] Pietsch U, Grenzer J, Geue Th, Neissendorfer F, Brezsesinski G, Symietz Ch, Mohwald H and Gudat W 2001 *Nucl. Instrum. Methods Phys. Res.* A **467** 1077
[10] Parratt L G 1954 *Phys. Rev.* **95** 359
[11] Wang W-H, Bai H Y, Zhang M, Zhao J H, Zhang X Y and Wang W K 1999 *Phys. Rev.* B **59** 10811
[12] Endo Y, Oikawa K, Miyazaki T, Kitakami O and Shimada Y 2003 *J. Appl. Phys.* **94** 7222
[13] Stavroyiannis S, Christides C, Niarchos D, Kehagias Th, Komninou Ph and Karakostas Th 1998 *J. Appl. Phys.* **84** 6221
[14] Fullerton E, Schuller I K, Vanderstraeten H and Bruynseraede Y 1992 *Phys. Rev.* B **45** 9292
[15] Fullerton E, Kumar S, Grimsditch M, Kelly D M and Schuller I K 1993 *Phys. Rev.* B **48** 2560
[16] Takayama T and Matsumoto Y 1990 *Advances in X-Ray Analysis* vol 33, ed C S Barrett, J V Gilfrich, T C Huang, R Jenkins and P K Predecki (New York: Plenum) p 109
[17] Cullity B D 1978 *Elements of X-Ray Diffraction* (London: Addison-Wesley)
[18] Stearns M B 1988 *Phys. Rev.* B **38** 8109
[19] Loirat Y, Boequet J L and Limoge Y 2000 *J. Non-Cryst. Solids* **265** 252
[20] Qiu Z Q and Bader S D 2000 *Rev. Sci. Instrum.* **71** 1243
[21] Hesse J, Nolle G and Korner H 1983 *Solid State Commun.* **46** 721
[22] Shinjo T and Keune W 1999 *J. Magn. Magn. Mater.* **200** 598